Nanoscale Rings Fabricated Using Self-Assembled Triblock Terpolymer Templates

Vivian P. Chuang,[†] Caroline A. Ross,[†,*] Panayiotis Bilalis,[‡] and Nikos Hadjichristidis[‡]

[†]Department of Materials Science and Engineering, Massachusetts Institute of Technology, Cambridge, Massachusetts 02139, and [‡]Department of Chemistry, University of Athens, Panepistimiopolis Zografou, 157 71 Athens, Greece

ABSTRACT Although there has been extensive work on the use of self-assembled diblock copolymers for nanolithography, there are few reports of the use of multiblock copolymers, which can form a more diverse range of nanoscale pattern geometries. Pattern transfer from a self-assembled poly(butadiene-*b*-styrene-*b*-methyl methacrylate) (PB-*b*-PS-*b*-PMMA) triblock terpolymer thin film has been investigated. Polymers of different total molecular weight were synthesized with a predicted morphology consisting of PMMA-core/PS-shell cylinders in a PB matrix. By adjusting the solvent-annealing conditions and the film thickness, thin films with vertically oriented cylinders were formed. The PMMA cylinder cores and the PB matrix were then removed using selective etching to leave an array of PS rings, and the ring pattern was transferred into a silica film by reactive ion etching to form 19 nm high silica rings. This result illustrates the design and use of triblock terpolymers for self-assembled lithography.

KEYWORDS: triblock polymers · lithography · self-assembly · thin films · nanoscale rings

The self-assembly of diblock copolymers into periodic nanoscale domains has attracted a great deal of interest because the resulting patterns may be used as nanolithographic templates.[1−8] This method offers the ability to pattern large area substrates with structures of controlled morphology and a periodicity of ~20−100 nm. Thin films of diblock copolymers have been used to pattern nanodot and nanowire arrays of semiconductors, oxides, and metals,[1−5] and devices such as capacitors, patterned magnetic storage media, and transistors.[6−8]

One of the main challenges in block copolymer lithography is to create a set of essential pattern geometries from which complex devices may be formed, such as sets of parallel lines, lines with angles (L-shapes), junctions (T-shapes), and square arrays of dots. Diblock copolymers (dBCPs), which microphase separate into spheres, cylinders, gyroids, or lamellae in the bulk, have been used to form well-ordered arrays of nanoscaled lines and dots,[9−11] single rows of ellipses,[12] or crossed lines[13,14] by self-assembly on substrates with chemical or topographical templates created using electron beam lithography. In addition to dot and line structures, a number of devices make use of ring-shaped features, for example, memories,[15,16] sensors,[17] transistors and quantum devices,[18,19] and structures for persistent current phenomena.[20] It is therefore of interest to create ring-shaped patterns by self-assembly of a block copolymer, as well as the lines and dots already achieved. Although ring structures do not occur in a bulk untemplated dBCP, concentric cylinders formed by lamellar dBCPs[21,22] and helical structures formed by cylindrical dBCPs[23,24] have been demonstrated by self-assembly of dBCPs within 3D templates such as narrow pores. However, pattern transfer from these 3D structures may be difficult. Ring and rod morphologies have been demonstrated in polystyrene-*b*-poly(4-vinyl pyridine) (PS-*b*-P4VP) in a mixture of water and toluene, but the rings are randomly distributed and mixed with rods.[25] Rings have also been made by self-assembly of a cylindrical dBCP in circular pits,[26] and a wide range of patterns has been fabricated using directed assembly of a blended dBCP on chemically patterned substrates,[27,28] but these methods require fabrication of appropriate templates.

In contrast, ring structures may be formed without templating by the self-assembly of more complex block copolymers such as the linear ABC triblock terpolymers. In such materials, a diversity of new structures can be obtained by designing the combination of block sequence, the interaction parameter between the adjacent blocks, and the volume fraction and molecular weights of the three blocks.[29,30] The experimental and theoretical work on ABC triblock terpolymers deals mainly with the

*Address correspondence to caross@mit.edu.

Received for review April 21, 2008 and accepted August 27, 2008.

Published online September 11, 2008.
10.1021/nn8002345 CCC: $40.75

© 2008 American Chemical Society

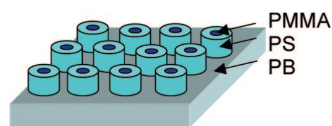

Figure 1. Concentric cylinder morphology triblock terpolymer PB-*b*-PS-*b*-PMMA.

bulk morphology,[31−39] but there has been some study of the complex structures generated by microphase separation of triblock terpolymer thin films.[40−50] For example, highly ordered perforated lamellae were formed in films of poly(styrene-*b*-2-vinyl pyridine-*b*-*tert*-butyl methacrylate) (PS-*b*-P2VP-*b*-PtBMA),[40,41] and well-ordered nanoporous thin films were made from poly-(ethylene oxide-*b*-methyl methacrylate-*b*-styrene) (PEO-*b*-PMMA-*b*-PS).[46] Moreover, nanopores with controlled pore wall functionality were fabricated by removing the core domains in core−shell structured triblock terpolymers,[47] while structures containing highly ordered perpendicular lamellae were made by application of an electric field to a triblock terpolymer with a short middle block.[49] Finally, a ring array in a poly(isoprene-*b*-styrene-*b*-lactide) (PI-*b*-PS-*b*-PLA) thin film has been demonstrated, where the PI and PLA were removed to leave PS rings.[50]

Despite this progress in understanding triblock thin film morphologies, there has been relatively little work on the use of triblock terpolymers as lithographic templates for pattern transfer. Here we show that an array of rings can be formed in poly(butadiene-*b*-styrene-*b*-methyl methacrylate) (PB-*b*-PS-*b*-PMMA) thin films. The terpolymer was synthesized by sequential anionic polymerization and spin-coated to form the geometry shown in Figure 1. The PMMA and PB blocks were then removed to leave the ring-shaped PS domains, and this pattern was transferred into a silica film. Silica rings may then serve as a mask for further pattern transfer into a functional material.

The polymers used here were designed using two criteria. First, the interaction parameters and volume fractions of the blocks were chosen to generate a bulk morphology expected to consist of an array of core−shell cylinders. Core−shell cylinders will occur in an ABC triblock terpolymer if C is the major block, which forms the matrix surrounding the cylinders, and if $\chi(A-C) > \chi(B-C) > \chi(A-B)$,[51] where χ is the segment−segment chemical interaction (Flory−Huggins) parameter, which is proportional to the difference between the solubility parameters of the components (blocks).[52] In the PB-*b*-PS-*b*-PMMA system, the solubility parameters of PS, PB, and PMMA are 18.5, 17, and 19 $(MPa)^{1/2}$, respectively.[53] Since PB-PMMA has the largest positive interaction parameter (the least favorable),[42] this polymer is expected to order into periodic core−shell cylinders if PB is the major block. The core−shell structures would consist of a PMMA core and a PS shell in a PB matrix. The second criterion is that the blocks should be removable with high selectivity, so that one or more blocks can be removed without degrading the morphology. In this work, we use a high percentage of 1,4 addition PB which can be etched using ozone to react with the double bond in the polymer backbone. These design considerations may be extendable to the formation of other triblock terpolymer thin film morphologies for lithographic applications.

RESULTS AND DISCUSSION

$PB_{1,4}$-*b*-PS-*b*-PMMA Triblock Terpolymer Characteristics. For these experiments, three different $PB_{1,4}$-*b*-PS-*b*-PMMA triblock terpolymers were synthesized with molecular weights 141, 179, and 185 kg/mol (Table 1), labeled BSM^{141}, BSM^{179}, and BSM^{185}. This is the first report of the synthesis of this triblock terpolymer. Although the synthesis of $PB_{1,4}$ -*b*-PS-*b*-PMMA is much more difficult than that of $PB_{1,2}$-*b*-PS-*b*-PMMA, it was necessary for lithographic processing because $PB_{1,4}$ can be removed more easily with ozonolysis compared to $PB_{1,2}$. Figure 2a shows a representative example (BSM^{141}) of size-exclusion chromatography (SEC) monitoring during the synthesis of the BSM triblock terpolymers. The polydispersity index (M_w/M_n) of the intermediate and final products is extremely low (PDI = 1.05), and no extra peaks, indicating deactivation of living chains, are apparent. The molecular weights of the intermediate and final products were determined by low-angle light scattering and are listed in Table 1. A representative ^1H NMR spectrum for BSM^{141} is shown in Figure 2b. The PS aromatic protons appear between 6.3 and 7.5 ppm, the methyl protons of PMMA are displayed at 3.6 ppm, whereas the characteristic PB protons resonate at 5 ppm (2 protons for $PB_{1,2}$) and 5.4 ppm (2 protons for $PB_{1,4}$ and 1 proton for $PB_{1,2}$).

Thin Film Orientation and Morphology. From the volume fractions and χ parameters of the blocks, the bulk mor-

TABLE 1. Volume Percentages (v/v %), Polydispersity (PDI), and Weight Percentages (w/w %) of the Three Triblock Terpolymers[a]

sample	Φ_{PB} % v/v	Φ_{PS} % v/v	Φ_{PMMA} % v/v	PDI	$PB_{1,2}$ % w/w	$PB_{1,4}$ % w/w	PS % w/w	PMMA %w/w
$B_{85}S_{40}M_{16}{}^{141}$	62.7	27.4	9.9	1.05	14.7	45.7	28.0	11.6
$B_{111}S_{36}M_{32}{}^{179}$	64.7	19.6	15.7	1.04	7.9	54.3	20.3	17.5
$B_{101}S_{55}M_{29}{}^{185}$	57.1	29.0	13.8	1.05	6.2	48.4	29.7	15.7

[a]Based on densities of PB: 0.9 g/cm^3, PS: 1.07 g/cm^3, and PMMA: 1.19 g/cm^3. In $B_xS_yM_z{}^w$, *x*, *y*, and *z* denote the blocks' molecular weights and *w* denotes the total molecular weight.

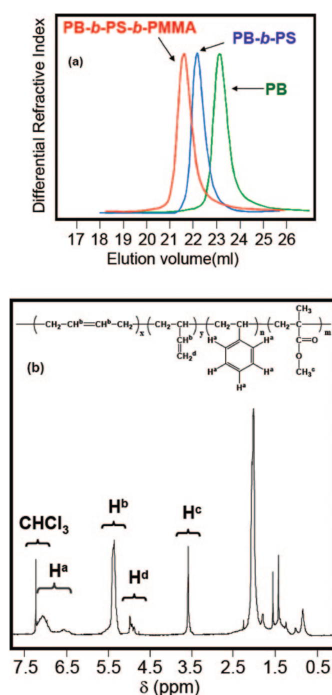

Figure 2. (a) SEC chromatogram of the intermediate compounds and final PB-*b*-PS-*b*-PMMA triblock terpolymer BSM[141]; (b) ^{1}H NMR of the $PB_{1,4}$-*b*-PS-*b*-PMMA triblock terpolymer BSM[141]. The blocks in the chemical structure labeled *x* and *y* indicate 1,2 and 1,4 PB, respectively.

phology of the terpolymers is expected to consist of PMMA cylinders with a PS shell in a PB matrix. Although the bulk morphology was not analyzed directly, images of the thin films, described below, show that this morphology was formed under the processing conditions used in this work. In order to use these terpolymers as lithography masks for making ring arrays, the cylinders must be oriented perpendicular to the film plane. This orientation can be accomplished by a combination of film thickness control and solvent annealing of the film after spin-casting.[50] During solvent annealing, the polymer film absorbs the solvent and swells. Upon removal from the solvent atmosphere, the concentration of the solvent in the film next to the free surface decreases, creating a concentration gradient normal to the surface, and this becomes the ordering front as the solvent evaporates from the film.[54] Furthermore, the process can be controlled by choice of solvent. For example, the vapor pressure for acetone at room temperature (181 Torr) is much higher than that of toluene (22 Torr), and as a result, the degree of swelling is higher for acetone than that for toluene[55] and the rapid evaporation of acetone promotes perpendicular cylinder formation due to kinetic constraints.[56] Compared to toluene, acetone has a strong preferential affinity for the PMMA block[57] while PB (32 mJ/m^2) and PS (40.7 mJ/m^2) have lower surface energy than PMMA (41.1 mJ/m^2).[58] The balance between selectivity of the solvent and surface energy of the swollen blocks can also promote the formation of perpendicular cylinders.[59] Thus, solvent annealing was used both to induce microphase separation in the polymer films and to promote orientation of the cylinders perpendicular to the film plane.

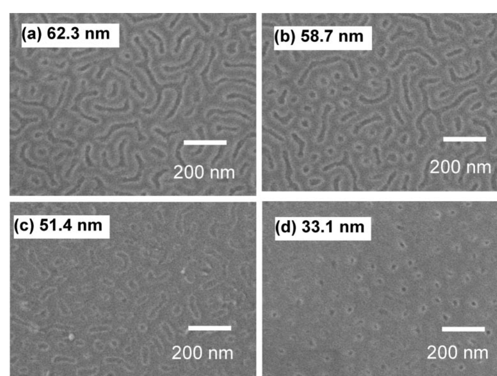

Figure 3. SEM images of thin films of BSM[179] with different thicknesses (labeled) after annealing in toluene vapor for 17.5 h at room temperature, followed by exposure with deep UV and etching with oxygen RIE to remove the PMMA, then etching with UV/O_3 and water to remove PB. The as-spun film thicknesses were (a) 62.3 nm, (b) 58.7 nm, (c) 51.4 nm, and (d) 33.1 nm.

Figure 3 shows the effect of film thickness on the morphology of BSM[179] films, which were annealed in toluene vapor then etched using deep UV exposure and oxygen reactive ion etching to remove the PMMA, then with UV/ozone and water to remove the PB. At 33.1 nm thickness, the cylinders are oriented perpendicular to the film, but as the thickness increases to 51 nm, a mixed orientation is formed, and at 62.3 nm, short in-plane cylinders are observed. The formation of in-plane cylinders is expected in films thicker than about half the domain periodicity.[54] Our terpolymers have periods of ~65−90 nm, so the observations are consistent with this expectation. The high molecular weights lead to poor ordering kinetics, and the cylinders form poorly ordered arrays.

The period of the cylinder arrays was measured from SEM images of etched films such as those shown in Figure 3. The period represents the average center-to-center spacing of perpendicular cylinders or the spacing measured normal to the cylinders for cylinders oriented in-plane. Each data point represents the average of approximately 20 measurements, and the standard deviation was of the order of ~7% of the period. The period was found to be sensitive to film thickness but insensitive to the solvent-annealing conditions. For example, Figure 4 shows the period of BSM[179] as a function of film thickness. The period is approximately 78 nm for films with thickness of 50−65 nm, a thickness range within which in-plane cylinders form, but increases for film thicknesses below 43 nm when perpendicular cylinders form. Similarly, the period of BSM[185] decreases from 80 to 68 nm as the thickness increases from 38.8 to 42.4 nm. However, the period is independent (within ~2 nm) of the choice of toluene, tetrahydrofuran, or acetone solvent vapor for a given thickness.

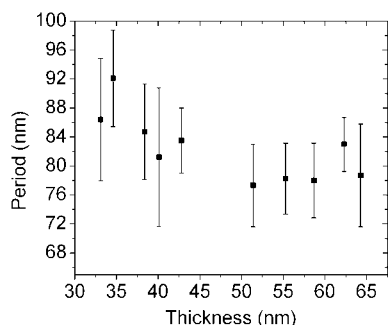

Figure 4. Period of the cylindrical domains in BSM[179] as a function of thickness. The error bars show one standard deviation.

TABLE 2. Period and Dimensions of PS Ring Patterns in Films of the Three Triblock Terpolymers after Annealing in Toluene Vapor Followed by Deep UV Exposure and Oxygen Etching[a]

	BSM[141]	BSM[179]	BSM[185]
film thickness (nm)	42.4	42.8	43.0
period (nm)	66 ± 5	82 ± 8	86 ± 7
inner ring diameter (nm)	11 ± 2	12 ± 2	15 ± 2
outer ring diameter (nm)	44 ± 4	56 ± 7	55 ± 5

[a]The data are based on the average of approximately 20 measurements from several SEM images including those of Figure 5.

Thickness-dependent cylinder spacing has been observed in other systems, for example, by Knoll *et al.*[60] for in-plane cylindrical PS-*b*-PB diblock copolymers. This was attributed to a competition between the surface energy and strain energy of the microdomains.

Figure 5 shows images of etched BSM films. The thickness of each film was within the range where perpendicular cylinders form and corresponds to 42.4, 42.8, and 43.0 nm for BSM[141], BSM[179], and BSM[185], respectively. The three triblock terpolymers exhibit differences in both period and microdomain inner and outer diameters, as shown in Table 2. The BSM[185] period is largest. Its period exceeds that of BSM[179], despite the similarity in their molecular weights, which is attributed to the fact that the sum of the volume ratios of the PS and PMMA blocks in BSM[185] is larger than that of BSM[179]. This phenomenon has been observed in other systems; for example, a larger period and larger diameter cylindrical domains were obtained in PS-*b*-PB-*b*-PMMA[94] (SBM[94]) compared to SBM[120] because the sum of the volume ratio of the minor components in SBM[94] was larger.[37]

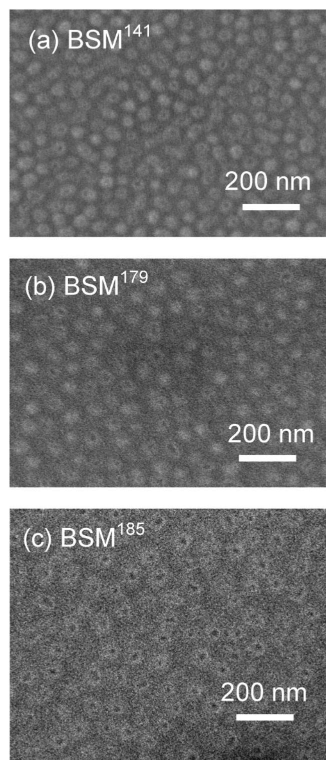

Figure 5. SEM images of thin films of PB-*b*-PS-*b*-PMMA: (a) MW = 141 kg/mol, (b) MW = 179 kg/mol, (c) MW = 185 kg/mol after annealing in toluene vapor, then UV exposure and etching with oxygen plasma.

Selective Etching of the PS, PB, and PMMA Blocks. The etch selectivity among the three blocks is one of the essential considerations for lithographic applications. As illustrated in Figure 3, in the PB-*b*-PS-*b*-PMMA triblock terpolymer, deep UV exposure degrades the PMMA domains and subsequent oxygen RIE removes the degraded PMMA to reveal the spatial arrangement of hollow PS cylinders in the PB matrix. In addition, a UV/ozone treatment degrades the 1,4 addition in the PB matrix by breaking the carbon−carbon double bonds in the polymer backbone. The UVO_3 process, which generates ozone and atomic oxygen from the interaction between UV radiation and oxygen, has been widely used in the microelectronics industry to remove organic contamination.[61,62] The degraded PB can be simply washed away by immersing in water.[1] Thus, in the end, one is left with PS rings, which can be used as a lithographic mask.

To quantify the etch selectivity, we begin by analyzing the etch rate of homopolymer PB, PS, and PMMA (hPB, hPS, and hPMMA) thin films under several etching conditions. Thin films of hPB (10.7 kg/mol molecular weight) with 19% 1,2 addition, hPS (17.5 kg/mol), and hPMMA (10.5 kg/mol) were spin-coated on silicon substrates with initial thicknesses of 55.1−58.3, 52.5−56.9, and 42.5−44.5 nm, respectively. After different etch protocols, the change in film thickness was measured. The thickness of each homopolymer film that was removed is given in Table 3 for a range of etch conditions. hPMMA has the highest etch rate for each etching condition, suggesting that PMMA can be removed with good selectivity compared to PS and PB. The maximum etch selectivity between hPMMA and hPS was obtained by including a UVO_3/water process step at 50 °C. However, the 50 °C water process leads to the production of stable intermediate compounds in hPB,[63] and the UV process can cause cross-linking of the 19% 1,2-PB present in hPB, making hPB more etch resistant. There was considerably less etch selectivity between hPB and hPS, with the hPS often etching at a similar rate to the hPB. The best process to remove hPMMA and hPB while leaving the hPS unaffected was protocol B in Table 3, which involved the use of deep UV exposure followed by a UVO_3/water process step at 50 °C.

Pattern Transfer into Silica. The results in the previous section demonstrate conditions under which hPMMA and hPB etch faster than hPS, as required for the formation of PS rings from the triblock terpolymer. However, when applying these etch methods to our triblock terpolymers, we found that the PMMA block could not be removed as easily as the results on the homopolymer suggest. For example, UVO_3/water was found to be ineffective by itself in removing the PMMA cores of the cylinders, and composite disks of PS/PMMA instead of rings of PS were obtained after an UVO_3/water treatment.

TABLE 3. Etching of Homopolymer PS (hPS), hPB, and hPMMA under Different Etching Conditions[a].

	etch method	etched thickness of hPMMA (nm)	etched thickness of hPS (nm)	etched thickness of hPB (nm)
A	A. (i) DUV exposure + O_2 RIE 11 s	16.2	5.5	7.8
	(ii) followed by UV/O_3 90 s + water @ 50 °C	26.3	3	2.2
B	B. (i) DUV exposure followed by UV/O_3 90 s + water @ 50 °C	42.5	0	3.7
C	(i) UV/O_3 90 s + water @ 50 °C	30.6	4.7	9.4
	(ii) followed by O_2 RIE 12 s		9.3	11.2
D	(i) O_2 RIE 11 s	16.9	6.2	7.7
	(ii) followed by UV/O_3 90 s + water @ 50 °C	10.6	1.4	1.6
	(iii) followed by 3 repeats of UV/O_3 90 s + water @ 50 °C	--	9.4	6.8
	(iv) followed by UV/O_3 90 s + CHF_3 RIE 180 s	--	10.2	12.2

[a]The thickness of each film removed by each etch step is given in nanometers. The initial thicknesses of the films were in the range of 44−58 nm. The dashes indicate where the etch thickness could not be measured because the film was mostly or completely etched by previous steps.

Several methods based on the results in Table 3 were explored to etch the terpolymer and to subsequently transfer the pattern from the polymer to the underlying silica film, three of which will be described here for BSM^{179}. In the first method, PMMA was removed by deep UV exposure and oxygen RIE, then the PB was etched using UVO_3/water treatment, then the PS pattern was etched into the silica layer using CHF_3 RIE. However, the PB was only partly removed by the UVO_3/water treatment, leading to incomplete transfer of the ring pattern (Figure 6a). There are three possible reasons for this. First, the 1,2 addition in the PB matrix may have been cross-linked under the deep UV exposure.[64] Second, after multiple or long-term UVO_3/water treatment, extended ozonation may have led to nonselective etching, causing the loss of the original cylindrical features.[65] Third, the PS features may not extend completely through the film due to the strong affinity of PMMA and PB for the silicon dioxide.[66,67]

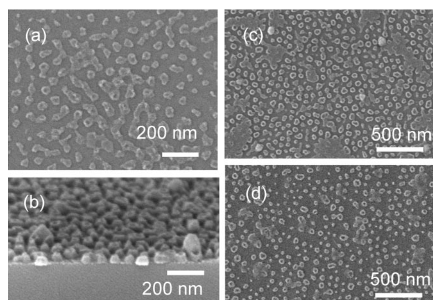

Figure 6. Pattern transfer into silica rings from a BSM^{179} film annealed in acetone vapor for 6 h. (a) The PMMA was removed with deep UV exposure and O_2 RIE, the PB with UV/ozone and water treatment, then the PS pattern was etched into the silica using CHF_3 RIE. The PB was only partially removed, leading to interconnected features, and overetching with CHF_3 causes missing rings. (b) Side view of PS-topped silica rings after a sequence of deep UV exposure, UVO_3/water (2×), CHF_3 RIE for 2.75 min, and an additional UVO_3/water treatment to remove the PMMA and PB, then a CHF_3 RIE for 1.85 min to transfer the pattern into silica. (c) Plan view of PS-topped silica rings after a sequence of deep UV exposure, UVO_3/water (3×), a short oxygen RIE, and a CHF_3 RIE for 2.75 min. (d) Plan view of silica rings after the sequence in (c) with an additional CHF_3 RIE for 0.85 min and oxygen RIE to remove the PS, leaving only the pattern in the silica.

The second pattern transfer method is to omit the deep UV exposure and oxygen RIE and instead use only the UVO_3/water treatment followed by CHF_3 RIE. The problem of cross-linking in the PB matrix is not an issue in this case. However, discrete dots instead of rings were formed in the silica layer since the PS and PMMA are both etched only slowly by the UVO_3/water treatment. Ozone attacks the in-chain double bond of PB, but PS has no double bonds in the polymer chain, and it is degraded about six times more slowly than PB in ozone. The C═O bond in the PMMA is more resistant to ozone attack than the C═C bond, so it is even more stable than polystyrene.[68,69]

The third method is to use only deep UV exposure followed by UVO_3/water, then a combined CHF_3 RIE and UVO_3/water treatment. The cross-sectional SEM image in Figure 6b shows a PS-capped silica ring array. The pattern can also be transferred by applying a short oxygen RIE before the CHF_3 RIE (Figure 6c,d). Figure 6c shows a plan view of PS-capped silica rings, and Figure 6d shows silica rings after removing the PS rings by oxygen RIE. In this process, the UV exposure time also plays an important role. Underexposure leads to interconnected dots and rings, while overexposure gives isolated but partly missing rings.

In Figure 6b−d, we see that the 20 nm thick PS ring array was transferred into 19 nm thick SiO_2 rings. However, compared to the etched BSM^{179} film (Figure 5a), the quality and uniformity of the silica pattern is degraded. For example, in Figure 6d, only about 80% of the PS rings transferred into silica features, and of these, only about 25% are rings instead of dots. In the etched BSM^{179} film, the average period, outer ring diameter, and inner ring diameter of the PS block after PB and PMMA removal were 83, 41, and 15 nm, respectively. For the silica ring pattern, measurements of just the ring-shaped features gave average values of 85, 48, and 18 nm, respectively. The poor uniformity of the silica rings is attributed partly to poor uniformity of the PS domains in the etched film and partly to degradation of the PS features during pattern transfer. The quality of the etched pattern may be improved by using a more

etch-resistant block chemistry in place of the PS, for example, an organometallic or Si-containing block such as poly(ferrocenyldimethylsilane) or poly(dimethylsiloxane), both of which have high etch resistance under an oxygen plasma and can serve as a good etch mask for transferring the pattern into silica.[11,70]

CONCLUSION

Cylindrical core–shell morphology thin films were obtained from $PB_{1,4}$-*b*-PS-*b*-PMMA triblock terpolymers with total molecular weights of 141, 179, and 185 kg/mol synthesized by anionic polymerization. Thin films of the polymers were formed by spin-coating and annealed to form self-assembled arrays of core–shell cylinders oriented perpendicular to the surface. The PMMA core and PB matrix blocks were removed using sequential etching, and the remaining PS ring pattern was transferred into an underlying silica film to form ring features. Pattern transfer from a 179 kg/mol molecular weight polymer led to a pattern of silica rings with a height of 19 nm, although the quality of the silica ring pattern was degraded compared to that of the triblock terpolymer.

EXPERIMENTAL METHODS

Synthesis and Characterization of $PB_{1,4}$-*b*-PS-*b*-PMMA Triblock Terpolymers. The polymer synthesis and almost all the purification techniques were performed under vacuum, in all-glass reactors provided with break-seals and constrictions. The purification of the monomers (1,3-butadiene, styrene, methyl methacrylate), 1,1-diphenylethylene (DPE), the solvents (THF and benzene), and the terminating agent MeOH was carried out according to literature methods.[71] The initiator *sec*-butyl lithium (*s*-BuLi) was prepared under vacuum from *sec*-butyl chloride and lithium metal in hexane.[72] In a typical experiment shown in Scheme 1 (described here for $PB_{1,4}$-*b*-PS-*b*-PMMA with a molecular weight of 141 kg/mol, or BSM^{141}), 70 mL of benzene was distilled into the polymerization apparatus, then 3.8 g of 1,3-butadiene was poured into the reactor flask, followed by addition of 0.047 mmol *s*-BuLi, by breaking the corresponding break-seal. The polymerization was allowed to proceed until complete consumption of the monomer (24 h). A small sample of the living PB was then removed, by flame sealing, for characterization.

A small amount of THF (0.5 mL) was added into the solution, followed by styrene (1.9 g), and the reaction was allowed to proceed for 24 h. After the polymerization was completed, 0.18 mmol of DPE (3-fold excess over the concentration of the living anions) was added. The solution was collected into an ampule equipped with a break-seal which was removed from the apparatus by flame sealing. A small amount of the living PB-*b*-PS was used for characterization. The ampule was attached to another apparatus where 210 mL of THF (THF/benzene = 3/1) was distilled and then the apparatus was subsequently sealed off from the vacuum line. The flask was cooled to −78 °C in a dry ice–2-propanol bath. The break-seal of the ampule containing the living PB-*b*-PS end-capped with DPE was broken, and the polymerization of methyl methacrylate was initiated by breaking the methyl methacrylate ampule (0.5 g) and distilling the monomer into the reactor. The polymerization was conducted for 1 h under vigorous mixing using a glass stirrer. Finally the living polymer was deactivated by adding degassed methanol. The polymer was precipitated in excess methanol. The final product was dried in a vacuum oven until constant weight. Three PB-*b*-PS-*b*-PMMA terpolymers, BSM^{141}, BSM^{179}, and BSM^{185}, of molecular weights 141, 179, and 185 kg/mol, respectively, were synthesized (Table 1).

To characterize the intermediate compounds, size-exclusion chromatography (SEC) experiments were conducted at 40 °C using a modular instrument consisting of a Waters model 510 pump, a Waters model U6K sample injector, a Waters model 401 differential refractometer, a Waters model 486 UV spectrometer, and a set of 4 μ-Styragel columns with a continuous porosity range from 10^6 to 10^3 Å. Tetrahydrofuran was the carrier solvent at a flow rate of 1 mL/min. Dual-detector SEC analysis [refractive index and two angle laser light scattering (SEC-TALLS) detectors], using a Waters 1525 high-pressure liquid chromatography pump, Waters Ultrastyragel columns (HR-2, HR-4, HR-5E, and HR-6E), a Waters 2410 differential refractometer detector, and a Precision 2020 two-angle (15°, 90°) light-scattering detector, was also employed for the determination of the refractive index increments, dn/dc, and the weight-average molecular weights of the samples. The ^{1}H NMR spectra were recorded in chloroform-*d* at 25 °C with a Varian Unity Plus 300/54 NMR spectrometer.

Thin Film Deposition and Characterization. The thin film samples were prepared by spin coating of 1 wt % toluene solution of PB-*b*-PS-*b*-PMMA to form films with thickness of 33–62 nm, as determined by ellipsometry. Substrates consisted of SiO_2(19 nm)/Cu(2 nm)/Co(9 nm)/Si substrate, in which the layers were deposited by electron beam evaporation. After annealing in acetone vapor for 5–6 h or toluene vapor for 17 h at room temperature, various etching steps were applied in order to remove the PB and PMMA domains completely before transferring the PS pattern into the silica layer. Deep UV exposure in an OAI (Optical Associates Inc.) exposure system using a wavelength of 220 nm and power of 0.48 μw for 320 or 500 s and oxygen reactive ion etching (RIE, in a Plasmatherm etcher) were primarily used to etch the PMMA. The PB was etched using UV/ozone, which attacks the double bonds of the 1,4 addition, then the samples were immersed in deionized

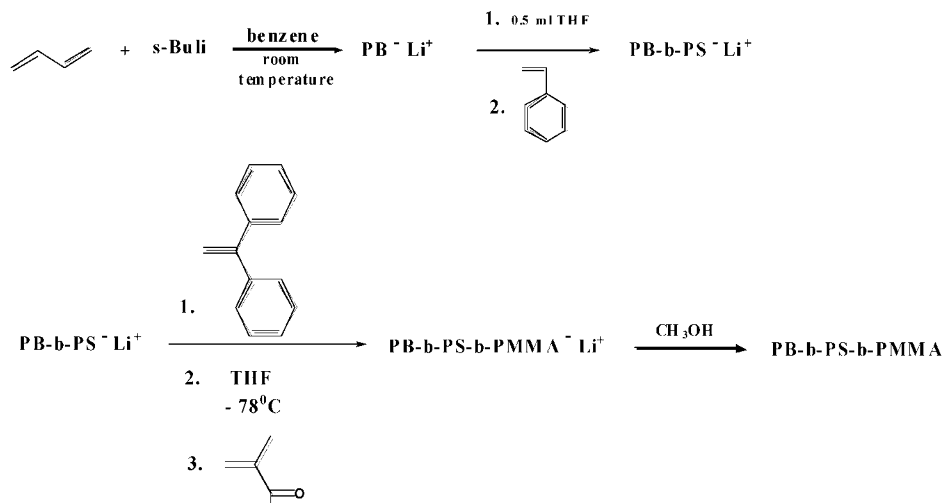

Scheme 1. Experimental pathway for the synthesis of $PB_{1,4}$-*b*-PS-*b*-PMMA triblock terpolymers.

water at room temperature or at 50 °C to wash away the degraded PB. The PS patterns were transferred into silica using a CHF_3 RIE.

Acknowledgment. V.P.C. and C.A.R. gratefully acknowledge the support of the Semiconductor Research Corporation and the Singapore−MIT Alliance.

REFERENCES AND NOTES

1. Park, M.; Harrison, C.; Chaikin, P. M.; Register, R. A.; Adamson, D. H. Block Copolymer Lithography: Periodic Arrays of ~10^{11} Holes in 1 Square Centimeter. *Science* **1997**, *276*, 1401–1404.
2. Li, R. R.; Dapkus, P. D.; Thompson, M. E.; Jeong, W. G.; Harrison, C.; Chaikin, P. M.; Register, R. A.; Adamson, D. H. Dense Arrays of Ordered GaAs Nanostructures by Selective Area Growth on Substrates Patterned by Block Copolymer Lithography. *Appl. Phys. Lett.* **2000**, *76*, 1689–1691.
3. Lammertink, R. G. H.; Hempenius, M. A.; Chan, V. Z.-H.; Thomas, E. L.; Vancso, G. J. Poly(ferrocenyldimethylsilanes) for Reactive Ion Etch Barrier Applications. *Chem. Mater.* **2001**, *13*, 429–434.
4. Cheng, J. Y.; Ross, C. A.; Chan, V. Z. H.; Thomas, E. L.; Lammertink, R. G. H.; Vancso, G. J. Formation of a Cobalt Magnetic Dot Array *via* Block Copolymer Lithography. *Adv. Mater.* **2001**, *13*, 1174–1178.
5. Thurn-Albrecht, T.; Schotter, J.; Kästle, G. A.; Emley, N.; Shibauchi, T.; Krusin-Elbaum, L.; Guarini, K.; Black, C. T.; Tuominen, M. T.; Russell, T. P. Ultrahigh-Density Nanowire Arrays Grown in Self-Assembled Diblock Copolymer Templates. *Science* **2000**, *290*, 2126–2129.
6. Black, C. T.; Guarini, K. W.; Milkove, K. R.; Baker, S. M.; Russell, T. P.; Tuominen, M. T. Integration of Self-Assembled Diblock Copolymers for Semiconductor Capacitor Fabrication. *Appl. Phys. Lett.* **2001**, *79*, 409–411.
7. Naito, K.; Hieda, H.; Sakurai, M.; Kamata, Y.; Asakawa, K. 2.5-in. Disk Patterned Media Prepared by an Artificially Assisted Self-Assembling Method. *IEEE Trans. Magn.* **2002**, *38*, 1949–1951.
8. Black, C. T. Self-Aligned Self Assembly of Multi-Nanowire Silicon Field Effect Transistors. *Appl. Phys. Lett.* **2005**, *87*, 163116.
9. Cheng, J. Y.; Mayes, A. M.; Ross, C. A. Nanostructure Engineering by Templated Self-Assembly of Block Copolymers. *Nat. Mater.* **2004**, *3*, 823–828.
10. Zschech, D.; Kim, D. H.; Milenin, A. P.; Scholz, R.; Hillebrand, R.; Hawker, C. J.; Russell, T. P.; Steinhart, M.; Gösele, U. Ordered Arrays of <100>-Oriented Silicon Nanorods by CMOS-Compatible Block Copolymer Lithography. *Nano Lett.* **2007**, *7*, 1516–1520.
11. Jung, Y. S.; Ross, C. A. Orientation-Controlled Self-Assembled Nanolithography Using a Polystyrene-Polydimethylsiloxane Block Copolymer. *Nano Lett.* **2007**, *7*, 2046–2050.
12. Cheng, J. Y.; Zhang, F.; Chuang, V. P.; Mayes, A. M.; Ross, C. A. Self-Assembled One-Dimensional Nanostructure Arrays. *Nano Lett.* **2006**, *6*, 2099–2103.
13. Kim, H.-C.; Cheng, J.; Rettner, C.; Park, O.-H.; Miller, R.; Hart, M.; Sundström, L.; Zhang, Y. Self-Aligned, Self-Assembled Organosilicate Line Patterns of ~20nm Half-Pitch from Block Copolymer Mediated Self-Assembly. *Proc. SPIE* **2007**, *6519*, 65191H.
14. Kim, S. O.; Kim, B. H.; Meng, D.; Shin, D. O.; Koo, C. M.; Solak, H. H.; Wang, Q. Novel Complex Nanostructure from Directed Assembly of Block Copolymers on Incommensurate Surface Patterns. *Adv. Mater.* **2007**, *19*, 3271–3275.
15. Castaño, F. J.; Morecroft, D.; Jung, W.; Ross, C. A. Spin-Dependent Scattering in Multilayered Magnetic Rings. *Phys. Rev. Lett.* **2005**, *95*, 137201.
16. Podbielski, J.; Giesen, F.; Grundler, D. Spin-Wave Interference in Microscopic Rings. *Phys. Rev. Lett.* **2006**, *96*, 167207.
17. Miller, M. M.; Prinz, G. A.; Cheng, S. F.; Bounnak, S. Detection of a Micron-Sized Magnetic Sphere Using a Ring-Shaped Anisotropic Magnetoresistance-Based Sensor: A Model for a Magnetoresistance-Based Biosensor. *Appl. Phys. Lett.* **2002**, *81*, 2211–2213.
18. Aharonov, Y.; Bohm, D. Significance of Electromagnetic Potentials in the Quantum Theory. *Phys. Rev.* **1959**, *115*, 485–491.
19. Yu, L. W.; Chen, K. J.; Song, J.; Xu, J.; Li, W.; Li, X. F.; Wang, J. M.; Huang, X. F. New Self-Limiting Assembly Model for Si Quantum Rings on Si(100). *Phys. Rev. Lett.* **2007**, *98*, 166102.
20. Lévy, L. P.; Dolan, G.; Dunsmuir, J.; Bouchiat, H. Magnetization of Mesoscopic Copper Rings: Evidence for Persistent Currents. *Phys. Rev. Lett.* **1990**, *64*, 2074–2077.
21. Sevink, G. J. A.; Zvelindovsky, A. V.; Fraaije, J. G. E. M.; Huinink, H. P. Morphology of Symmetric Block Copolymer in a Cylindrical Pore. *J. Chem. Phys.* **2001**, *115*, 8226–8230.
22. Xiang, H.; Shin, K.; Kim, T.; Moon, S. I.; McCarthy, T. J.; Russell, T. P. Block Copolymers under Cylindrical Confinement. *Macromolecules* **2004**, *37*, 5660–5664.
23. Yu, B.; Sun, P. C.; Chen, T. C.; Jin, Q. H.; Ding, D. T.; Li, B. H.; Shi, A. C. Confinement-Induced Novel Morphologies of Block Copolymers. *Phys. Rev. Lett.* **2006**, *96*, 138306.
24. Xiang, H.; Shin, K.; Kim, T.; Moon, S. I.; McCarthy, T. J.; Russell, T. P. From Cylinders to Helices upon Confinement. *Macromolecules* **2005**, *38*, 1055–1056.
25. Pietsch, T.; Gindy, N.; Fahmi, A. Preparation and Control of Functional Nano-Objects: Spheres, Rods and Rings Based on Hybrid Materials. *Polymer* **2008**, *49*, 914–921.
26. Jung, Y. S.; Jung, W.; Ross, C. A. Nanofabricated Concentric Ring Structures by Templated Self-Assembly of a Diblock Copolymer *Nano Lett.* **2008**, 10.1021/nl070924l.
27. Stoykovich, M. P.; Kang, H. K.; Daoulas, C.; Liu, G.; Liu, C.; de Pablo, J. J.; Müller, M.; Nealey, P. F. Directed Self-Assembly of Block Copolymers for Nanolithography: Fabrication of Isolated Features and Essential Integrated Circuit Geometries. *ACS Nano* **2007**, *1*, 168–175.
28. Daoulas, K. C.; Müller, M.; Stoykovich, M. P.; Park, S. M.; Papakonstantopoulos, Y. J.; de Pablo, J. J.; Nealey, P. F. Fabrication of Complex Three-Dimensional Nanostructures from Self-Assembling Block Copolymer Materials on Two-Dimensional Chemically Patterned Templates with Mismatched Symmetry. *Phys. Rev. Lett.* **2006**, *96*, 036104.
29. Bates, F. S.; Fredrickson, G. H. Block Copolymers-Designer Soft Materials. *Phy.s Today* **1999**, *52*, 32–38.
30. Abetz, V.; Simon, P. F. W. Phase Behaviour and Morphologies of Block Copolymers. *Adv. Polym. Sci.* **2005**, *189*, 125–212.
31. Hadjichristidis, N.; Iatrou, H.; Pitsikalis, M.; Pispas, S. Avgeropoulos, Linear and Non-linear Triblock Terpolymers. Synthesis, Self-Assembly in Selective Solvents and in Bulk. A. *Prog. Polym. Sci.* **2005**, *30*, 725–782.
32. Takahashi, K.; Hasegawa, H.; Hashimoto, T.; Bellas, V.; Iatrou, H.; Hadjichristidis, N. Four-Phase Triple Coaxial Cylindrical Microdomain Morphology in a Linear Tetrablock Quaterpolymer of Styrene, Isoprene, Dimethylsiloxane, and 2-Vinylpyridine. *Macromolecules* **2002**, *35*, 4859–4861.
33. Brinkmann, S.; Stadler, R.; Thomas, E. L. New Structural Motif in Hexagonally Ordered Cylindrical Ternary (ABC) Block Copolymer Microdomains. *Macromolecules* **1998**, *31*, 6566–6572.
34. Ludwigs, S.; Böker, A.; Abetz, V.; Müller, A. H. E.; Krausch, G. Phase Behavior of Linear Polystyrene-*block*-Poly(2-vinylpyridine)-*block*-Poly(*tert*-butyl methacrylate) Triblock Terpolymers. *Polymer* **2003**, *44*, 6815–6823.
35. Gido, S. P.; Schwark, D. W.; Thomas, E. L.; Goncalves, M. C. Observation of a Non-Constant Mean Curvature Interface in an ABC Triblock Copolymer. *Macromolecules* **1993**, *26*, 2636–2640.
36. Krappe, U.; Staler, R.; Martin, I. V. Chiral Assembly in Amorphous ABC Triblock Copolymers. Formation of a Helical Morphology in Polystyrene-block-polybutadiene-

ARTICLE

block-poly(methyl methacrylate) Block Copolymers. *Macromolecules* **1995**, *28*, 4558–4561.

37. Breiner, U.; Krappe, U.; Abetz, V.; Stadler, R. Cylindrical Morphologies in Asymmetric ABC Triblock Copolymers. *Macromol. Chem. Phys.* **1997**, *198*, 1051–1083.
38. Jung, K.; Abetz, V.; Stadler, R. Thermodynamically Controlled Morphological Disorder in a Microphase-Separated Cylindrical Block Copolymer. *Macromolecules* **1996**, *29*, 1076–1078.
39. Breiner, U.; Krappe, U.; Jakob, T.; Abetz, V.; Stadler, R. Spheres on Spheres—A Novel Spherical Multiphase Morphology in Polystyrene-*block*-Polybutadiene-*block*-Poly(methyl methacrylate) Triblock Copolymers. *Polym. Bull.* **1998**, *40*, 219–226.
40. Ludwigs, S.; Böker, A.; Voronov, A.; Rehse, N.; Magerle, R.; Krausch, G. Self-Assembly of Functional Nanostructures from ABC Triblock Copolymers. *Nat. Mater.* **2003**, *2*, 744–747.
41. Sperschneider, A.; Schacher, F.; Gawenda, M.; Tsarkova, L.; Müller, A. H. E.; Ulbricht, M.; Krausch, G. Köhler, Towards Nanoporous Membranes Based on ABC Triblock Terpolymers. *Small* **2007**, *3*, 1056–1063.
42. Stocker, W.; Beckmann, J.; Stadler, R.; Rabe, J. P. Surface Reconstruction of the Lamellar Morphology in a Symmetric Poly(styrene-*block*-butadiene-*block*-methyl methacrylate) Triblock Copolymer: A Tapping Mode Scanning Force Microscope Study. *Macromolecules* **1996**, *29*, 7502–7507.
43. Elbs, H.; Drummer, C.; Abetz, V.; Krausch, G. Thin Film Morphologies of ABC Triblock Copolymers Prepared from Solution. *Macromolecules* **2002**, *35*, 5570–5577.
44. Böker, A.; Müller, A. H. E.; Krausch, G. Nanoscopic Surface Patterns from Functional ABC Triblock Copolymers. *Macromolecules* **2001**, *34*, 7477–7488.
45. Elbs, H.; Abetz, V.; Hadziioannou, G.; Drummer, C.; Krausch, G. Antiferromagnetic Ordering in a Helical Triblock Copolymer Mesostructure. *Macromolecules* **2001**, *34*, 7917–7919.
46. Bang, J.; Kim, S. H.; Drockenmuller, E.; Misner, M. J.; Russell, T. P.; Hawker, C. J. Defect-Free Nanoporous Thin Films from ABC Triblock Copolymers. *J. Am. Chem. Soc.* **2006**, *128*, 7622–7629.
47. Rzayev, J.; Hillmyer, M. A. Nanoporous Polystyrene Containing Hydrophilic Pores from an ABC Triblock Copolymer Precursor. *Macromolecules* **2005**, *38*, 3–5.
48. Aizawa, M.; Buriak, J. M. Nanoscale Patterning of Two Metals on Silicon Surfaces Using an ABC Triblock Copolymer Template. *J. Am. Chem. Soc.* **2006**, *128*, 5877–5866.
49. Olszowka, V.; Hund, M.; Kuntermann, V.; Scherdel, S.; Tsarkova, L.; B̈; oker, A; Krausch, G. Large Scale Alignment of a Lamellar Block Copolymer Thin Film via Electric Fields: A Time-Resolved SFM Study. *Soft Matter* **2006**, *2*, 1089–1094.
50. Guo, S.; Rzayev, J.; Bailey, T. S.; Zalusky, A. S.; Olayo-Valles, R.; Hillmyer, M. A. Nanopore and Nanobushing Arrays from ABC Triblock Thin Films Containing Two Etchable Blocks. *Chem. Mater.* **2006**, *18*, 1719–1721.
51. Sugiyama, M.; Shefelbine, T. A.; Vigild, M. E.; Bates, F. S. Phase Behavior of an ABC Triblock Copolymer Blended with A and C Homopolymers. *J. Phys. Chem. B* **2001**, *105*, 12448–12460.
52. Nagarajan, R.; Barry, M.; Ruckenstein, E. Unusual Selectivity in Solubilization by Block Copolymer Micelles. *Langmuir* **1986**, *2*, 210–215.
53. Barton, A. F. M. *CRC Handbook of Polymer−Liquid Interaction Parameters and Solubility Parameters*; CRC Press: Boca Raton, FL, 1990; p 297.
54. Kim, S. H.; Misner, M. J.; Xu, T.; Kimura, M.; Russell, T. P. Highly Oriented and Ordered Arrays from Block Copolymers via Solvent Evaporation. *Adv. Mater.* **2004**, *16*, 226–231.
55. Elbs, H.; Krausch, G. Ellipsometric Determination of Flory−Huggins Interaction Parameters in Solution. *Polymer* **2004**, *45*, 7935–7942.
56. Kim, G.; Libera, M. Morphological Development in Solvent-Cast Polystyrene-Polybutadiene-Polystyrene (SBS) Triblock Copolymer Thin Films. *Macromolecules* **1998**, *31*, 2569–2577.
57. Xuan, Y.; Peng, J.; Cui, L.; Wang, H.; Li, B.; Han, Y. Morphology Development of Ultrathin Symmetric Diblock Copolymer Film via Solvent Vapor Treatment. *Macromolecules* **2004**, *37*, 7301–7307.
58. Mark, J. E. *Physical Properties of Polymer Handbook*; AIP Press: New York, 1996; pp 405−406.
59. Cavicchi, K. A.; Berthiaume, K. J.; Russell, T. P. Solvent Annealing Thin Films of Poly(isoprene-*b*-lactide). *Polymer* **2005**, *46*, 11635–11639.
60. Knoll, A.; Tsarkova, L.; Krausch, G. Nanoscaling of Microdomain Spacings in Thin Films of Cylinder-Forming Block Copolymers. *Nano Lett.* **2007**, *7*, 843–846.
61. Wood, P. C.; Wydeven, T.; Tsuji, O. Critical Process Variables for UV-Ozone Etching of Photoresist. *Mater. Res. Soc. Symp. Proc.* **1993**, *315*, 237–242.
62. Kim, H.-C.; Kreller, C. R.; Tran, K. A.; Sisodiya, V.; Angelos, S.; Wallraff, G.; Swanson, S.; Miller, R. D. Nanoporous Thin Films with Hydrophilicity-Contrasted Patterns. *Chem. Mater.* **2004**, *16*, 4267–4272.
63. Zoller, D. L.; Johnston, M. V. Microstructures of Butadiene Copolymers Determined by Ozonolysis/MALDI Mass Spectrometry. *Macromolecules* **2000**, *33*, 1664–1670.
64. Von Raven, A.; Heusinger, H. Radiation-Induced Crosslinking and Cyclization in 1,2-Polybutadiene. *J. Polym. Sci. Polym. Chem. Ed.* **1974**, *12*, 2255–2271.
65. Collins, S; Hamley, I. W.; Mykhaylyk, T. Atomic Force Microscopy Study of Ozone Etching of a Polystyrene/Polyisoprene Block Copolymer. *Polymer* **2003**, *44*, 2403–2410.
66. Mayes, A. M.; Russell, T. P.; Bassereau, P.; Baker, S. M.; Smith, G. S. Evolution of Order in Thin Block Copolymer Films. *Macromolecules* **1994**, *27*, 749–755.
67. Harrison, C.; Park, M.; Chaikin, P. M.; Register, R. A.; Adamson, D. H.; Yao, N. Layer by Layer Imaging of Diblock Copolymer Films with a Scanning Electron Microscope. *Polymer* **1998**, *39*, 2733–2744.
68. Jeong, U.; Ryu, D. Y.; Kim, J. K.; Kim, D. H.; Russell, T. P.; Hawker, C. J. Volume Contractions Induced by Crosslinking: A Novel Route to Nanoporous Polymer Films. *Adv. Mater.* **2003**, *15*, 1247–1250.
69. Rimmer, S.; Ebdon, J. R. Synthesis of Telechelic Oligostyrenes by the Ozonoloysis of Poly(styrene-stat-butadiene): Protection of Styrene Units Against Ozone Attack by the Use of Di-*N*-alkyl Amides as Sacrificial Ozone Scavengers. *J. Polym. Sci. Part A: Polym. Chem.* **1996**, *34*, 3573–3583.
70. Cheng, J. Y.; Ross, C. A.; Chan, V. Z.-H.; Thomas, E. L.; Lammertink, R. G. H.; Vancso, G. J. Formation of a Cobalt Magnetic Dot Array *via* Block Copolymer Lithography. *Adv. Mater.* **2001**, *13*, 1174–1178.
71. Hadjichristidis, N.; Iatrou, H.; Pispas, S.; Pitsikalis, M. Anionic Polymerization: High Vacuum Techniques. *J. Polym. Sci. Part A: Polym. Chem.* **2000**, *38*, 3211–3234.
72. Uhrig, D.; Mays, J. W. Experimental Techniques in High-Vacuum Anionic Polymerization. *J. Polym. Sci. Part A: Polym. Chem.* **2005**, *43*, 6179–6222.